Radio-Over-Fiber 16-QAM, 100-km Transmission at 5 Gb/s Using DSB-SC Transmitter and Remote Heterodyne Detection

Chia-Kai Weng, Yu-Min Lin, and Winston I. Way, *Fellow, IEEE*

***Abstract*—By using a double-sideband suppressed carrier (DSB-SC) optical transmitter and a remote self-heterodyned (RSH) detection method, we experimentally and analytically proved the feasibility of a radio-over-fiber system using a 16-QAM signal at 5 Gb/s and 18 GHz, with a transmission distance of 100 km between a mobile service center and a base station. The transmission system performance was carefully analyzed by considering optical amplifier noise, fiber nonlinearity, phase noise, frequency response, and analog-to-digital converter (ADC) quantization noise. The 18-GHz, 16-QAM signal can be radiated from the base station to a remote antenna port without any upconverter, and the remote antenna port consists of a downconverter and high-speed digital signal processors (DSPs) to recover the 16-QAM signal. The high-speed DSP, which partially compensates the intersymbol-interference (ISI) and phase-noise-induced system penalties, was enabled by 20-Gs/s ADCs. The algorithms used in the DSP blocks were also described in details.**

***Index Terms*—Coherent detection, digital signal processing (DSP), double-sided suppressed carrier (DSB-SC), quadrature amplitude modulation (QAM), remote self-heterodyned (RSH) detection, subcarrier modulation (SCM).**

I. Introduction

In a radio-over-fiber system which carries millimeter-wave signals, the chromatic dispersion-limited transmission distance can be extended by using optical single-sideband modulation technique [1], whereas the radio-spectrum-limited capacity can be overcome by using multilevel modulation techniques such as *M*-ary quadrature amplitude modulation (M-QAM) techniques [2]–[4]. To transport multigigabit/s data, integrated optical vector modulator (IOVM) is a common method which has been proposed in coherent optical M-QAM systems [4]–[7]. It should be noted that traditional subcarrier multiplexed M-QAM system suffers from poor modulation efficiency, dispersion tolerance, and receiver sensitivity [2], while conventional coherent system is economically prohibitive. Therefore, a remote self-heterodyned (RSH) system could serve as an attractive alternative solution [8]–[10], which is the main subject to be analytically and experimentally investigated in this paper.

In this paper, we propose and demonstrate an optical transmitter based on double-sideband suppressed carrier (DSB-SC) [11], and an optical receiver based on digital-signal-processing (DSP) technique, to build an RSH system which transports multigigabit/s data rate using optical M-QAM. Furthermore, we verified an unrepeated 100-km transmission system with standard single-mode fiber (SSMF).

The paper is organized as follows. In Section II, the principle of operation for wideband QAM signal generation is described. In Section III, the fundamental performance for RSH is analyzed and the result is compared for coherent detection and SCM systems. In Section IV, the experimental results on a back-to-back and a 100-km transmission system are described. In Section V, the DSP technique which was used to improve the system performance degradation is described. Section VI concludes the paper.

Manuscript received August 24, 2007.

C.-K. Weng is with the Department of Communications Engineering, National Chiao-Tung University, Hsinchu, Taiwan, R.O.C. (e-mail: jack.nctu@gmail.com).

Y.-M. Lin is with Information and Communications Research Laboratories, Industrial Technology Research Institute, Hsinchu, Taiwan, R.O.C. (e-mail: ymlin@itri.org.tw).

W. I. Way is with OpVista Inc., Milpitas, CA 95035 USA (e-mail: wway@opvista.com).

Digital Object Identifier 10.1109/JLT.2007.912526

II. Principle of Operation

The proposed optical transmitter to generate a wideband optical QAM signal in an RSH system is shown in Fig. 1. A DSB-SC-modulator [11] is used to generate two wavelengths whose frequency and phase differences are tightly controlled through a microwave oscillator. The first wavelength, which serves as the local oscillator at the heterodyne receiver, is unmodulated and properly attenuated. The second wavelength is modulated by an integrated optical vector modulator (IOVM), which is composed of three modulators: a Mach-Zehnder modulator (MZM) for in-phase modulation (MZM_I), an MZM for quadratic-phase modulation (MZM_Q), and a phase modulator for controlling the phase difference between the MZM_I and MZM_Q [12]. To generate an optical 16 QAM signals, MZM_I and MZM_Q are both biased at a minimum transmission point and are modulated by two independent four-level pulse amplitude modulated (4-PAM) baseband nonreturn-to-zero (NRZ) signals, while the phase modulator maintains a 90° phase shift between the output signals of MZM_I and MZM_Q. The E-fields of the unmodulated and modulated wavelengths at the output of the QAM-RSH transmitter are given by

$$E_{LO}(t) = A\cos\left(\omega_{LO}t + \theta_{LO}(t)\right) \tag{1}$$

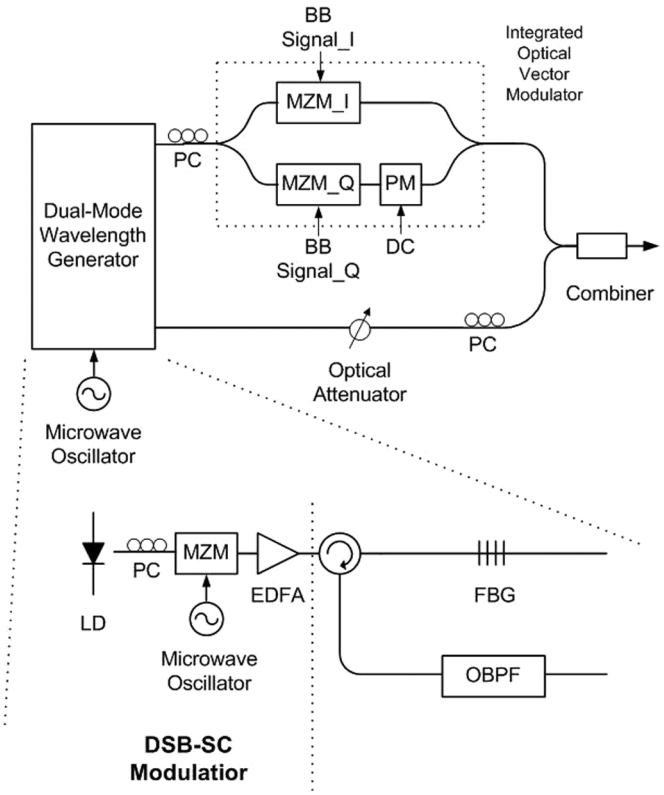

Fig. 1. QAM-Remote Heterodyne (QAM-RSH) transmitter configuration for the generation of a wideband optical QAM signal. BB Signal. I/Q: Baseband in-phase/quadratic-phase component of the QAM signal. DC: constant bias voltage. FBG: fiber Bragg grating. FPF: Fabry–Pérot filter.

and

$$E_S(t) = B\cdot[I'(t)\cos(\omega_S t + \theta_S(t)) + Q'(t)\sin(\omega_S t + \theta_S(t))] \tag{2}$$

respectively. In (1), A is the amplitude of the remote LO carrier, $\omega_{LO} = 2\pi(f_0 - (f_m/2))$ and $\theta_{\rm LO}(t)$ are the radian frequency and phase of the remote LO carrier, respectively; f_0 is the frequency of the laser diode, and $f_m/2$ is the frequency of the microwave oscillator. In (2), $I'(t) = \sin(\pi I(t)/2V_{\pi\_I})$ and $Q'(t) = \sin(\pi Q(t)/2V_{\pi\_Q})$, where $I(t) = \Sigma_n I_n p(t - nT_s)$ and $Q(t) = \Sigma_n Q_n p(t - nT_s)$ are the electrical m-PAM data for the in- and quadratic-phase components of a $2^{\rm m}$-QAM signal, respectively; $p(t)$ is a rectangular pulse signal with unit amplitude and time duration T_s; V_{π_I} and V_{π_Q} are the half-wave switching voltage of MZM_I and MZM_Q, respectively; $\omega_S = 2\pi(f_0 + (f_m/2))$ and $\theta_S(t)$ are the radian frequency and phase of the modulated signal. We assume that the $2^{\rm m}$-QAM signal has a uniform and rectangular constellation (m is an even number), and, therefore, the amplitude levels of the m-PAM must be properly adjusted to compensate for the nonlinear sinusoidal transfer function of the MZM_I and MZM_Q. For example, with $\pi I_n/2V_{\pi\_I} = (-0.5\pi, -0.108\pi, 0.108\pi, 0.5\pi)$, we obtain a uniformly distributed amplitude of $I'(t) = (-1, -1/3, 1/3, 1)$. Note that the polarization states of the two wavelengths are aligned through a polarization controller before they were recombined. Owing to the fact that the polarizations and frequencies of both modulated and unmodulated wavelengths are well controlled at a DSB-SC transmitter, an RSH receiver becomes significantly simpler than a coherent receiver.

A system diagram for a radio-over-fiber network using the proposed RSH technique is shown in Fig. 2. A QAM-RSH transmitter, located in a central office, sent an optical M-QAM signal together with a remote LO carrier through an optical fiber link with a total optical loss L. At a remote base station, both the modulated signal and reference carrier are amplified by an erbium-doped fiber amplifier (EDFA) with an optical gain G, filtered with an optical bandpass filter (OBPF) centered at f_0 and a 3-dB bandwidth of B_0, and received by a wideband direct-detection optical receiver. The detected signal after the wideband optical receiver is given by

$$\begin{aligned} I_r(t) &= R\left|\sqrt{GL}\,(E_s(t) + E_{LO}(t))\right|^2 \\ &= RGLAB\cdot[I'(t)\cos(2\pi f_m t + \Delta\theta(t)) \\ &\qquad -Q'(t)\sin(2\pi f_m t) + \Delta\theta(t))] \\ &\quad + DC\ terms. \end{aligned} \tag{3}$$

where R is the photodiode responsivity, and $\Delta\theta(t) = \theta_{LO}(t) - \theta_S(t)$. It can be seen from (3) that the in-phase modulating signal $I'(t)$ and quadratic-phase modulating signal $Q'(t)$, both at the beat frequency f_m, have been recovered. The microwave/millimeter-wave signal is then amplified and radiated via an antenna. At the remote antenna port, the received microwave/millimeter-wave signal is downconverted to an intermediate-frequency (IF) signal. The optical and electrical spectra are also shown in Fig. 2. Note that in a remote antenna port, an IF digital receiver [2], [4] is used.

III. System Performance Analysis

A. SNR Comparison of RSH, Coherent Detection, and SCM System

In this section, we would like to compare the SNR performances of transmission systems based on three different detection methods: RSH, coherent, and subcarrier-multiplexed (SCM) systems, all with an optical preamplifier. We assume that the transmitted signal and LO power at the output of the QAM-RSH transmitter in Fig. 2 are P_s and $P_{\rm LO}$, respectively. Considering only signal-spontaneous (Sig-Sp) and LO-Spontaneous (LO-Sp) beat noise, we have the IF SNR of an RSH system given by (measured with an electrical bandwidth B at the IF band)

$$\mathrm{SNR}_{\rm RSH,IF} = \frac{\frac{1}{2}(2RGL\sqrt{P_S P_{\rm LO}})^2}{2\eta R^2 LGS_{\rm ASE}(P_S + P_{\rm LO})\cdot B} \tag{4}$$

where $2\eta R^2 LGS_{\rm ASE}P_S$ and $2\eta R^2 LGS_{\rm ASE}P_{\rm LO}$ are the Sig-Sp and LO-Sp beat noise density, respectively, B is the IF filter bandwidth, $S_{\rm ASE} = 2n_{\rm eq}(G-1)h\nu$ is the ASE spectral noise density in two polarizations, $n_{\rm eq}$ is the equivalent spontaneous emission factor of the optical amplifier, $h\nu$ is the photon energy, and $\eta = 1$ or 1/2 depending on the optical filter bandwidth [13]. Here, $\eta = 1/2$ corresponds to the condition of image-rejecting filtering and is illustrated in Fig. 3.

It could be seen from Fig. 3 that, when the optical filter (centered at f_0) has a bandwidth $B_o < 3f_m - B$, the in-band noise can

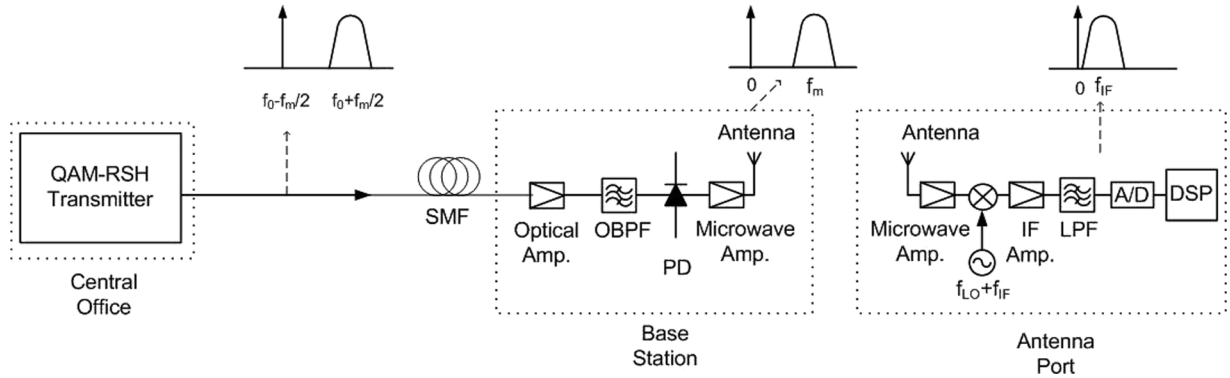

Fig. 2. System configuration for a radio-over-fiber system using the proposed RSH-QAM system. $\mathrm{DSP} = \mathrm{Digital\ Signal\ Processor}$.

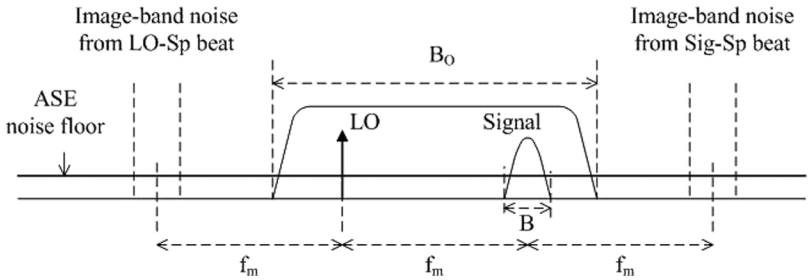

Fig. 3. Description of image-band noise rejection condition of OBPF.

be reduced by 3 dB due to the image-band LO-Sp and Sig-Sp noise rejection.

The maximum SNR at the demodulator output for RSH system, derived from (4) when $\mathrm{P_s} = \mathrm{P_{LO}}$ is then given by

$$\mathrm{SNR_{RSH,IF}} = \frac{\mathrm{LP_T}}{8\eta \cdot \mathrm{n_{eq}} \mathrm{h}\nu \mathrm{B}} \quad \text{for } \mathrm{G} \gg 1 \tag{5}$$

where $\mathrm{P_S} = \mathrm{P_{LO}} = \mathrm{P_T}/2$, and $\mathrm{P_T}$ is the total optical power at the transmitter output.

For coherent heterodyne detection based on a strong LO signal located at receiver, assuming the LO power is significantly greater than that of the amplified signal, the noise is dominated by LO-Sp beat noise, and the SNR at the output of a photodetector is given by

$$\mathrm{SNR_{coh}} = \frac{\frac{1}{2}(2R\sqrt{\mathrm{GLP}_S P_{\mathrm{LO}}})^2}{2\eta R^2 S_{\mathrm{ASE}} P_{\mathrm{LO}} B} = \frac{LP_T}{2\eta \cdot n_{\mathrm{eq}} h\nu B} \quad \text{for } \mathrm{G} \gg 1. \tag{6}$$

Note that $\mathrm{P_T} = \mathrm{P_S}$ for the coherent heterodyne system. It can be observed from (5) and (6) that for the same total transmission power, the maximum achievable SNR for coherent heterodyne detection based on a strong LO signal is 6 dB higher than that of RSH detection.

For a conventional subcarrier modulation system, its SNR is given by

$$\mathrm{SNR_{SCM}} = \frac{\frac{1}{2}(Rm_{\mathrm{rms}}\mathrm{GLP}_T)^2}{2R^2 S_{\mathrm{ASE}} \mathrm{GLP}_T B} = \frac{m_{\mathrm{rms}}^2 LP_T}{8n_{\mathrm{eq}} h\nu B} \quad \text{for } \mathrm{m} \ll 1 \tag{7}$$

where $\mathrm{m_{rms}}$ is the root-mean-square optical modulation index, and is typically less than 20%. For example, if $\mathrm{m_{rms}} = 10\%$, the SNR penalty of an SCM system is 23 dB when compared with an RSH system with $\mathrm{P_S} = \mathrm{P_{LO}}$ and $\eta = 1/2$, given that both systems have the same total transmission power and ASE noise floor. Fig. 4 shows the calculated SNR as a function of the total received power $(\mathrm{P_r} = \mathrm{LP_T})$ for the three transmission systems ($\mathrm{B} = 2.5$ GHz and $\mathrm{n_{eq}} = 2$). We can see that even though the RSH system has a 6–dB worse SNR performance than a conventional coherent system, it has a significant SNR advantage over conventional SCM systems.

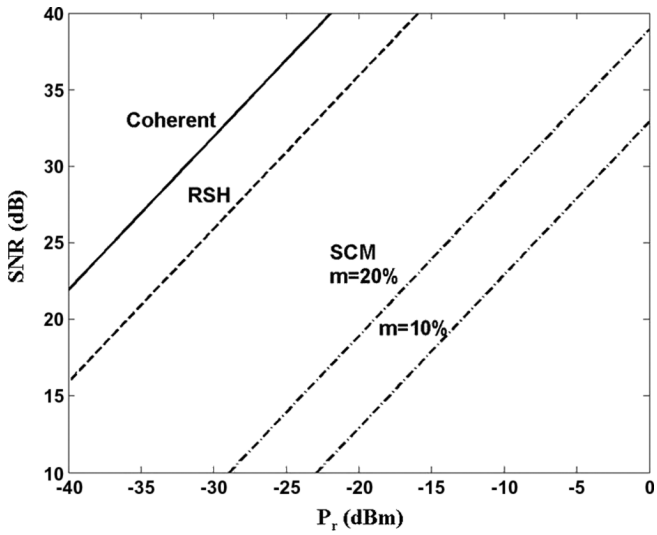

Fig. 4. Calculated results for coherent ($\eta = 1/2$), RSH ($\eta = 1/2$ with $\mathrm{P_S} = \mathrm{P_{LO}}$), and conventional SCM systems (with $\mathrm{m} = 10\%$ and 20%).

Note that the calculated results in Fig. 4 for SCM systems were based on a linear electrical-to optical (E-O) transfer function, and, therefore, a small error could be incurred for $\mathrm{OMI} = 20\%$ if the E-O transfer function is not linear. It should also

be noted that at OMI higher than 20%, the constellation was severely degraded because of the in-band nonlinear distortion, and the effect could not be evaluated simply from SNR measurement.

In our experiment, an actually measurable parameter called modulation error ratio (MER) was obtained. MER is defined as $\mathrm{MER} = (I_r^2+Q_r^2)/((I_r-I_o)^2+(Q_r-Q_o)^2)$, where I_r, Q_r are the demodulated in-phase and quadrature-phase symbols, and I_o, Q_o are the ideal normalized in-phase and quadrature-phase QAM symbols. Note that MER is equal to the baseband SNR [given in (10)] when only uniform additive white Gaussian noise (AWGN) is considered.

B. M-QAM RSH System Receiver Sensitivity

In this section, we would like to compare the receiver sensitivity of ASK, 4-QAM, 16-QAM, and 64-QAM modulations in an RSH system with an ideal preamplifier ($\mathrm{n_{eq}} = 1$), by using a bit-rate-independent figure of merit, i.e., the required photons per bit to achieve a bit-error ratio (BER) of 10^{-9}. Our analysis is based on the following assumptions: (1) synchronous demodulation [14] with a matched-filter being used; (2) $\mathrm{P_s} = \mathrm{P_{LO}}$; (3) $\eta = 1/2$; and (4) the noise variance for each constellation point is equal to the average noise variance. Assumption (4) implies that we do not consider the amplitude-dependent noise for QAM BER calculation. In our calculation and Monte Carlo simulation, however, amplitude-dependent noise could cause some excessive optical power penalty of ~1 dB for 16-QAM and ~1.4 dB for 64-QAM modulation when a midpoint threshold was used.

For ASK matched-filter demodulation, the BER is given by (see Appendix A)

$$\mathrm{BER_{ASK}} = \frac{1}{2} erfc\left(\sqrt{\frac{SNR_{D\_ASK}}{4}}\right) \tag{8}$$

where $\mathrm{SNR_{D\_ASK}}$ is the symbol signal-to-noise ratio (SNR) of the sampled matched-filter signal. The baseband $\mathrm{SNR_{D\_ASK}}$ is equal to IF SNR by letting $\mathrm{B} = \mathrm{R_S}/2 = \mathrm{R_b}/2$ in (5) and we have

$$\mathrm{SNR_{D\_ASK}} = \frac{LP_T}{2 \cdot n_{\mathrm{eq}} h\nu R_b} = \frac{n_b}{2} \tag{9}$$

where n_b is the average received photons per bit. To achieve a $\mathrm{BER} = 10^{-9}$, the required n_b for ASK modulation is then equal to 144. For a coherent heterodyne systems using synchronous detection, the required n_b is 36 [14], which is 6 dB superior to that of an RSH system.

To calculate the BER for a demodulated M-QAM signal, the symbol SNR ($\mathrm{SNR_{D\_QAM}}$) of the sampled matched-filter signal at baseband is first determined. The $\mathrm{SNR_{D\_QAM}}$ is equal to $\mathrm{SNR_{IF}}$ by letting $\mathrm{B} = 2(\mathrm{R_S}/2) = 2(\mathrm{R_b}/2\log_2 \mathrm{M})$ by considering only either in-phase or quadrature-phase component of the sampled matched-filter signal. The $\mathrm{SNR_{D\_QAM}}$ is then given by

$$SNR_{D\_QAM} = \frac{\log_2 MLP_T}{4 \cdot n_{eq} h\nu R_b} = \frac{\log_2 M n_b}{4} \tag{10}$$

The M-QAM signals can be decomposed into two independent $\sqrt{M}$-PAM signals. The error probability of these two $\sqrt{M}$-PAM signals is the same and could be treated independently. With Gray coded bit mapping and the assumption that errors occur between neighbor pairs in the constellation, the BER of a square-shaped M-QAM constellation over AWGN channel is derived from [15]. The BER for 4-, 16-, and 64-QAM modulation is then given by

$$\mathrm{BER_{4-QAM}} = \frac{1}{2} erfc\left(\sqrt{\frac{\mathrm{SNR_{D\_QAM}}}{2}}\right) \tag{11}$$

$$\mathrm{BER_{16-QAM}} = \frac{3}{8} erfc\left(\sqrt{\frac{\mathrm{SNR_{D\_QAM}}}{10}}\right) \tag{12}$$

$$\mathrm{BER_{64-QAM}} = \frac{7}{24} erfc\left(\sqrt{\frac{\mathrm{SNR_{D\_QAM}}}{42}}\right) \tag{13}$$

To achieve $\mathrm{BER} = 10^{-9}$, the required n_b for 4-, 16- and 64-QAM modulation are given by ~72 ($\mathrm{SNR_{D\_4QAM}} = 15.6$ dB), ~178 ($\mathrm{SNR_{D\_16QAM}} = 22.5$ dB) and ~489 ($\mathrm{SNR_{D\_64QAM}} = 28.7$ dB), respectively. Note that if we compare the 4- and 16-QAM results with those of [16], which shows the required photon numbers per bit are 18 and 45, respectively, we can clearly see the 6 dB receiver sensitivity advantage of a coherent heterodyne system. It is worth mentioning here that the ~6 dB higher SNRD requirement of 64-QAM than 16-QAM implies a higher ~6 dB OSNR in the optical transmission system and could present a significant challenge.

IV. Experiment

The experimental setup is essentially what we have shown in Figs. 1 and 2. The dual-wavelength signal generator was constructed via a DSB-SC transmitter with a modulating tone of 9 GHz. One of the wavelengths was filtered by a fiber grating (FBG) and sent into an X-cut $\mathrm{LiNbO_3}$ IOVM which consists of three modulating ports [12], two of which functioned as the interfaces to a pair of synchronized and independent 4-PAM signals. Each of these two ports had a half-wave switching voltage of ~5 V. The third port, a DC port with a half-wave switching voltage of ~6 V, was used to control a phase modulator. The other wavelength was reflected by the FBG, and passed through a Fabry–Pérot filter (FPF) to further suppress the unwanted spurious signals. This filtering configuration achieved more than 35 dB suppression of spurious signals for both wavelengths. The modulated and the unmodulated wavelengths were combined and heterodyned at a remote 20-GHz photodiode to generate a wideband QAM signal at 18 GHz. By using a microwave mixer and a local oscillator (LO) at 19.5 GHz, the 18-GHz signal was amplified and down converted to an IF frequency at 1.5 GHz. The 1.5-GHz IF signal was amplified and sampled by a high-speed digital oscilloscope (Tektronics TDS7404) with analog-to-digital converters (ADCs) running at 20 Gs/s. The amplitude of the IF signal was $\sim 400\ \mathrm{mV_{pp}}$. The amplitude level was optimal in the sense that the ADC was run at nearly a full scale and the quantization noise can be reduced without significant signal distortion. The digital data was stored and processed by an offline software based on Matlab program in the personal computer, similar to those used in [2], [4] and [17].

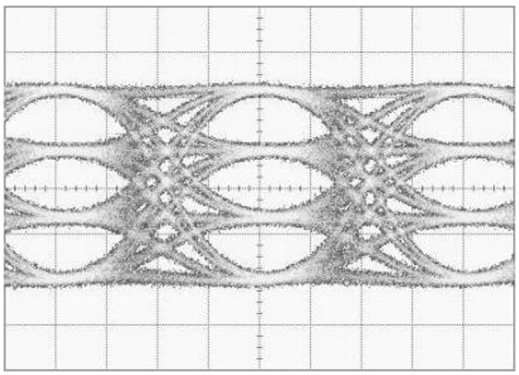

Fig. 5. Measured 4-PAM eye diagram at the output of the LPF.

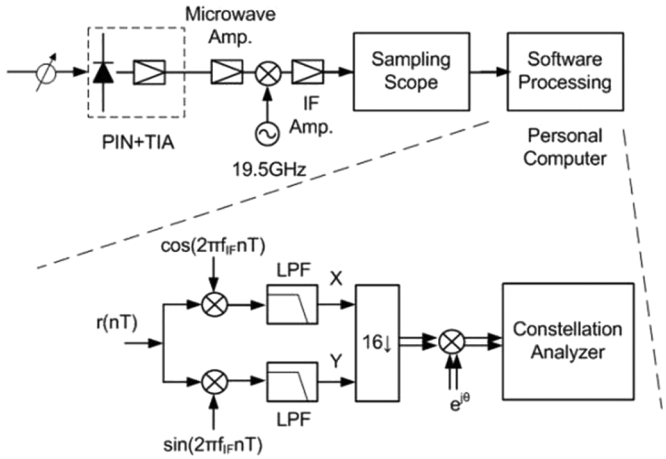

Fig. 6. Software processing of the IF data for demodulation.

Each of the two 4-PAM signals was generated by superimposing two binary NRZ signals with a proper amplitude adjustment to equalize the differences between any two adjacent power levels [18]. The binary NRZ data was 1.25 Gbps, which corresponds to 5 Gbps data rate for the 16-QAM signal. Note that each 4-PAM signal was formed by using the data and data-inverse outputs of a pulse pattern generator (PPG). The data and inverse-data outputs were decorrelated by a transmission cable, and the transmission-cable-induced delay was fine tuned via a mechanical delay line for symbol synchronization. The 4-PAM signal was then amplified and filtered by a linear-phase low-pass-filter (LPF) with a 3 dB-bandwidth of 930 MHz. The measured eye diagram at the LPF output is shown in Fig. 5. The peak-to-peak voltage of the 4-PAM signal was ~6 V, which corresponds to ~0.6 modulation index $(= V_{pp}/2\ V_{\pi\_I,Q})$. Note that to generate two 4-PAM signals synchronously, two PPGs operating in master and slave mode were used, and the symbol synchronization between the two PPGs was adjusted by the clock phase of the master PPG.

The IF data was downconverted by a digital I/Q mixer, and the I- and Q-components were subsequently separately filtered by a digital Raised-cosine filter with 3-dB bandwidth of 875 MHz and an alpha factor of 0.4, and re-sampled to keep one sample per symbol period with a decimation factor of 16 (20 GHz/1.25 GHz). Due to the different physical propagation lengths experienced by the modulated and unmodulated optical carriers, the phase difference between them caused the measured constellation rotated with an arbitrary phase. This phase rotation can be compensated by multiplying a complex phasor. A constellation analyzer, which computes the modulation error ratio (MER), was used to measure the link performance of the 5 Gbps 16-QAM signal [2]. The block diagram of the software demodulation is shown in Fig. 6.

The Fourier transformed power spectral density of the IF signal is shown in Fig. 7. The resolution bandwidth was 10 MHz, and the 20 dB bandwidth was ~2 GHz, which demonstrates an achievable spectral efficiency of ≥2.5 bits/Hz $(= 5\ \mathrm{Gb/s}/(2\ \mathrm{GHz}))$.

The measured constellation at the software constellation analyzer is shown in Fig. 8(a). Also shown in this figure are the ideal signal constellation and the decision boundaries for data decision. No error was observed in the window duration of 12.5 k

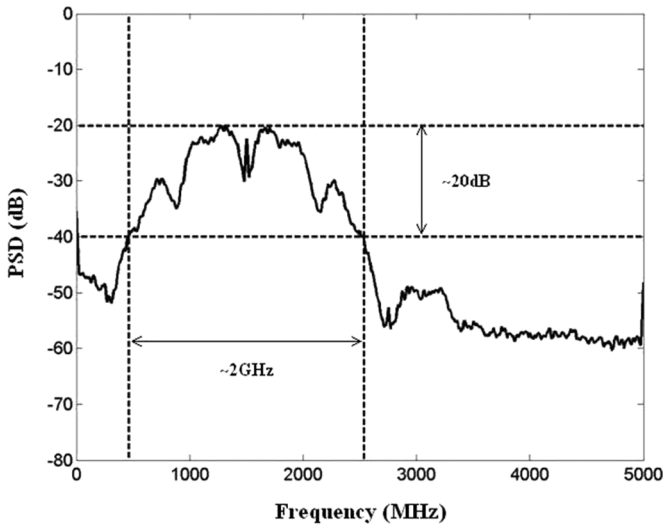

Fig. 7. Calculated power spectral density of the sampled IF signal.

symbols. The measured MER was 20.58 dB. It should be mentioned that the MER (or $\mathrm{SNR_{D\_QAM}}$) to achieve a $\mathrm{BER} = 10^{-9}$ is ~22.5 dB via (12).

An optical pre-amplifier was used before the 20 GHz photodetector, and its total optical power was controlled to be −6 dBm via a variable optical attenuator. The optical amplifier was followed by an optical bandpass filter (OBPF) with a 3-dB bandwidth of ~40 GHz. The optical spectrum showing the OBPF filter shape and the dual-wavelength signals are shown in Fig. 9.

A. Back-to-Back MER Measurement

The measured and calculated MER are shown in Fig. 10. The calculated total $\mathrm{MER_t}$ includes the optical pre-amplifier-limited $\mathrm{MER_{OA}}$, and the quantization noise-limited $\mathrm{MER_q}$. $\mathrm{MER_{OA}}$ is obtained from (5) with $\mathrm{n_{eq}} = 2$, $\mathrm{B} = \mathrm{R_S} = 1.25\ \mathrm{GHz}$, $\mathrm{LP_T} = \mathrm{P_r}$, and an η is between 1/2 and 1 due to the imperfect image rejection via the OBPF in the experiment. $\mathrm{MER_q}$ is given by $6.02 \times \mathrm{ENOB} + 1.76\ (\mathrm{dB})$, where ENOB is effective number of bits of the sampling scope's ADC and is equal to 5 in our experiment. It can be seen that

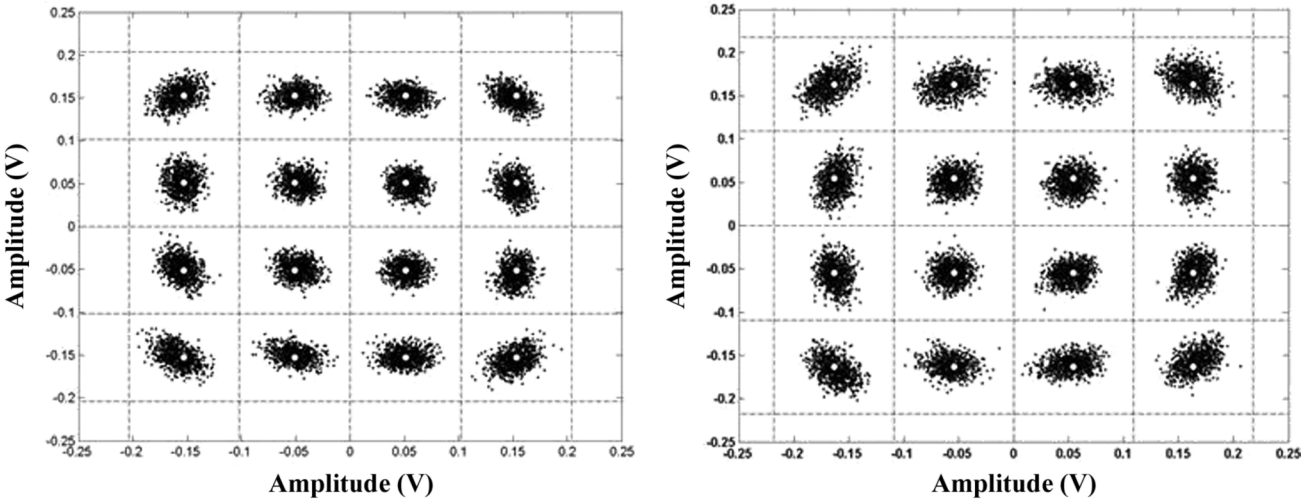

Fig. 8. Measured 16-QAM constellation diagram (a) back-to-back with $\mathrm{MER} = 20.58$ dB (b) 100 km transmission with 2 dBm launched power with $\mathrm{MER} = 20.24$ dB. The circle points represent the ideal signal constellation, and the dashed lines are the decision thresholds.

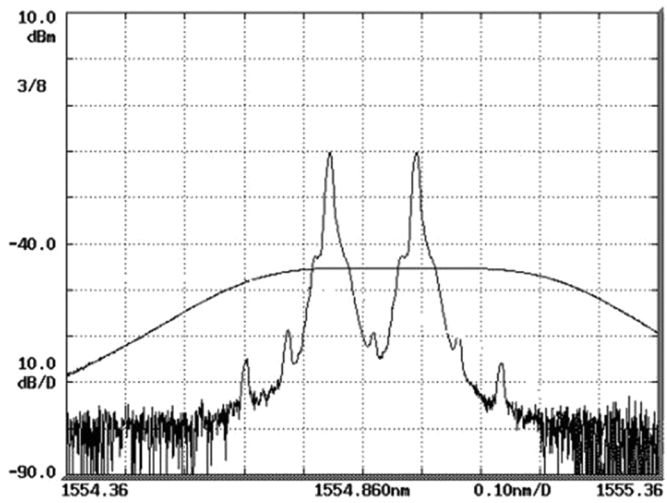

Fig. 9. Spectral shape of the OBPF and the spectrum of the dual-wavelength signals in the experiment. The shorter wavelength is the modulated optical carrier, and the longer wavelength is the unmodulated optical carrier. The spectral resolution of the optical spectrum analyzer was set at 0.01 nm.

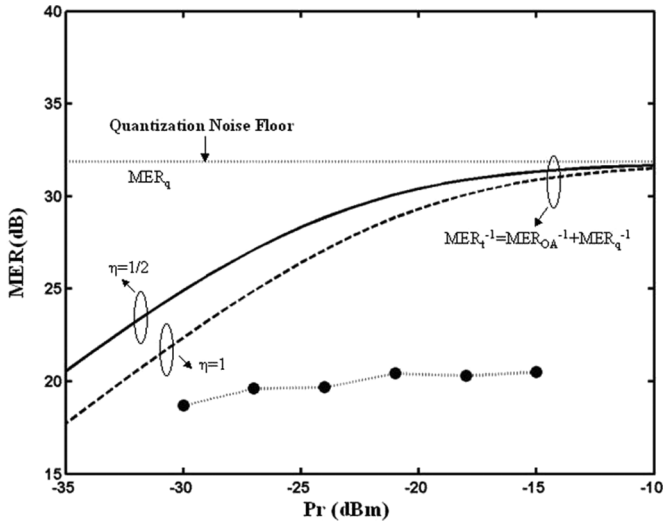

Fig. 10. MER dependence on optical amplifier input power: Solid circle points are the measured MER; solid and dashed lines are the calculated MER with and without the image rejection filter, respectively; dotted line is the ADC quantization noise-limited MER (with an ENOB of 5 bits).

the measured MER (circle points) is lower than the calculated $\mathrm{MER_t}$ by as much as $\sim$11 dB. This severe degradation is caused by the intersymbol interference (ISI) and phase noise, which will be discussed in Section V.

B. Unrepeated 100-km Transmission Experiment

After the back-to-back measurement of MER is done, a 100-km SMF-28 transmission fiber, and a booster-amplifier, were added to the experimental setup. The received optical power of the wideband photodetector was again fixed at -6 dBm.

The measured MER was 20.24 dB when the fiber input power was 2 dBm. The measured constellation is shown in Fig. 8(b). There is a smaller than 0.4 dB MER penalty compared to that of the back-to-back performance. Therefore, it is clear that the transmission performance is limited by the back-to-back setup, whose performance is limited by ISI and phase noise to be described in the next section.

V. Discussion

A. Effects of Phase Noise and Frequency Response

The effect of carrier phase noise is characterized by the same experiment setup as shown in Figs. 1 and 2. In order to get an independent phase measurement without data modulation, only DC signals are applied to the IOVM. The DC bias levels are adjusted and controlled in a manner that the I/Q ports of the IOVM are both biased at maximum transmission power. The received single-frequency IF signal was digitally I/Q downconverted, low-pass filtered, and its phase calculated via MATLAB program. By fitting the measured data to a Gaussian distribution,

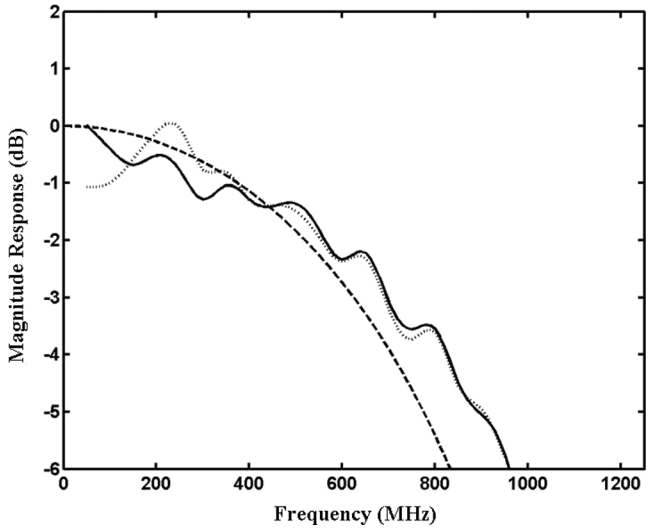

Fig. 11. Measured frequency response with (solid line) and without (dotted line) equalizer, and the ideal raised cosine filter response with roll-off factor of 1(dashed line).

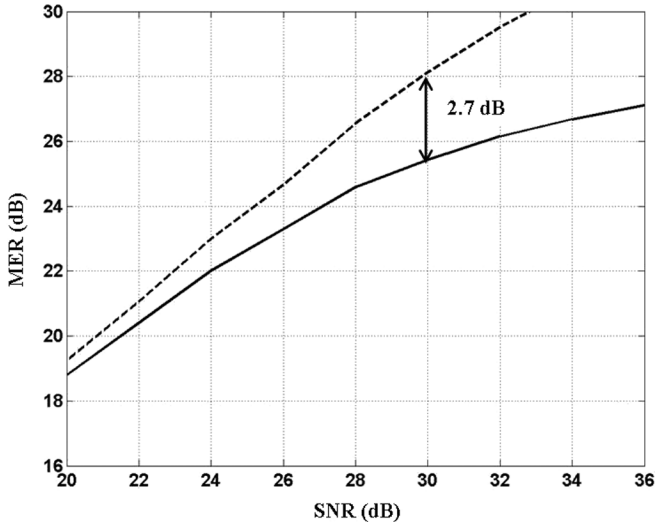

Fig. 12. Simulated result for MER dependence on SNR, considering only ISI effect due to the imperfect frequency response. Solid line represents the result without an equalizer. Dash line represents the result with the derived equalizer.

we found that the standard deviation $\sigma_{\rm p}$ of phase was $\sim$0.05 radians (2.86°). The total recorded number of samples was 12.5 k. The phase noise sources include: (a) the LO phase noise in the transmitter, (b) the phase difference between the modulated carrier and LO which propagated through the system with different transmission lengths, and (c) the 19.5 GHz LO (see Fig. 6) phase noise in the receiver. Note that the measured system SNR was very high (>30 dB) and, therefore, the impact of the amplitude noise was negligible in this phase noise characterization.

The MER penalty $\rm D_{phase}$ due to phase noise, which is the ratio of MER [at the presence of both phase noise and additive white Gaussian noise (AWGN)] and SNR (while only AWGN is presents), is given by [19] (approximated for $\sigma_{\rm p} \ll 1$)

$$D_{\rm Phase} = 10\log\left(1 + SNR \cdot \sigma_p^2\right) \tag{14}$$

For an SNR of 30 dB, $D_{\rm phase}$ is 5.44 dB, which is quite significant if the phase noise is left uncompensated.

The frequency response measurement setup is also the same by replacing the PPG with a microwave synthesizer at the input of the IF amplifier. The frequency of the output signal from the microwave synthesizer is changed from 50 MHz to 1250 MHz with a step of 50 MHz and the microwave synthesizer output power was used as a reference. The received sample of this single-frequency IF signal is then digitally I/Q downconverted, low pass filtered, and Fourier transformed by the offline processor, and the results are shown as the dotted line in Fig. 11. Note that the resultant power was calculated and normalized to the transmitted power at the corresponding frequency, and was the average measured results of I- and Q-channels (note that there is no significant difference between the I- and Q-channels). An ideal raised cosine filter with a roll-off factor of 1 is also shown in Fig. 11 for comparison. The nonideal frequency response would induce ISI on the QAM signal, and its effect was investigated through simulations by comparing the measured frequency responses with and without an equalizer (whose design will be described later). A low-pass equivalent model was used. The simulation results are shown as the solid line in Fig. 12. It is shown that, for $\rm SNR = 30\ dB$ (and, therefore, the system is not limited by SNR), the MER penalty due to ISI is $\sim$4.6 $(= 30 - 25.4)$ dB without the equalizer. The MER is limited to $\sim$27 dB even with $\rm SNR > 35\ dB$ without the equalizer because the ISI dominates the MER penalty.

B. Back-to-Back Performance Improvement Through ISI Equalization and Phase Tracking

In order to improve the back-to-back MER performance, we implemented a time-domain ISI equalizer and a phase tracking block, both within a Matlab-based demodulator, as is shown in Fig. 13. The detailed functions of the phase tracking block and ISI equalizer are described in the following sections.

ISI Equalization: The equalizer is designed to compensate the imperfect frequency response of the back-to-back system, and is not attempted to equalize the transmission-induced transfer function.

To compensate the ISI effect in the back-to-back system, an adaptive feed-forward equalizer (FFE) is applied to equalize the system response. The adaptive equalizer is based on the well-known least-mean-square (LMS) algorithm [20]. The equalizer has 128 taps with tap frequency equivalent to symbol rate, and is trained with the collected samples in a personal computer iteratively. With $\sim 10^5$ training symbols, the MER is converged and the filter coefficients are fixed in our experiment. It should be noted that the adaptive algorithm is only used to blindly compensate the static system transfer function; after the filter coefficients are converged we did not attempt to dynamically adjust it. The effect of the equalizer is illustrated in Fig. 12. We can see that there was $\sim$2.7 dB MER improvement at $\rm SNR = 30\ dB$ by using the equalizer.

Phase Error Correction: We used feed-forward decision directed (FF-DD) carrier phase recovery algorithm [21] for phase error correction. It has been shown that such algorithm realizes maximum-likelihood (ML) carrier phase estimation in an approximate form for high SNR. Unlike the traditional phase-

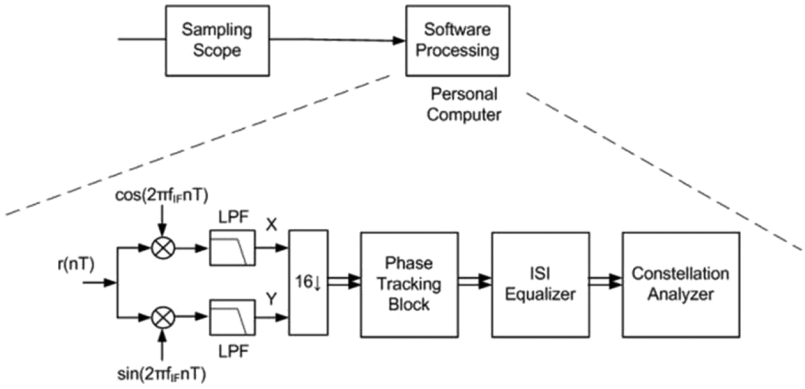

Fig. 13. Software processing for performance improvement through phase tracking block and ISI equalization.

locked loop (PLL) approach [7], [19], the feed-forward algorithm estimate the carrier phase directly through an explicit form without relying on one-dimension searching process iteratively provided by PLL. Hence, no loop delay is introduced which is very suitable for tracking the carrier phase generated by the beating of optical carriers, such as in coherent optical systems [17], and the DSP causes negligible processing latency. The FF-DD algorithm estimates the carrier phase for the *k*th block of symbols with the following form:

$$\hat{\theta}_k = \arg\left(\sum_{i=1}^{N} \hat{a}_k^*(i).z_k(i)\right) \tag{15}$$

where $\hat{\theta}_k$ is the ML carrier phase estimation for the *k*th block of symbols, $\hat{a}_k^*(i)$ is the complex conjugate of the *i*th decision output of the *k*th block of symbols derived from $\hat{\theta}_{k-1}$, $z_k(i)$ is the *i*th received symbol of the *k*th block, and *N* is the length of the block. The initial phase $(\hat{\theta}_0)$ would be estimated from the preamble bits in the acquisition stage of the phase recovery block. The decision on the *i*th symbol of the *k*th block is then updated after subtracting the carrier phase drift derived from the *k*th ML phase estimation:

$$\widetilde{a}_k(i) = DEC\left(z_k(i).e^{-j\hat{\theta}_k}\right) \tag{16}$$

where $\widetilde{a}_k(i)$ is the final decision output, and DEC() computes the decision metrics for M-QAM signals. It should be noted that the phase drift should not vary significantly over *NT*, where *N* is the block length and *T* is the symbol rate, in order to get a correct estimate. Note that a larger *N* can reduce the estimation error because the noise level is averaged over a larger time window, while a smaller *N* provides faster tracking of the carrier phase.

The resultant MER improvement due to the combined effect of ISI equalizer and phase error correction block is shown in Fig. 14. The case for MER improvement through only phase tracking block is shown with a dotted line for $\mathrm{N}=$125 and 25, respectively. The difference of MER between $\mathrm{N} = 125$ and 25 is not significant (The measured MER at $\mathrm{Pr} = -15$ dBm was 21.44 dB for $\mathrm{N} = 125$, and 21.78 dB for $\mathrm{N} = 25$). Note that higher N is preferred from the viewpoint of phase updating rate even though the required buffer size is larger; for example, in our experiment, $\mathrm{N} = 25$ stands for a phase updating rate of 50 MHz for 1.25 Gsps symbol rate, and stands for 10 MHz

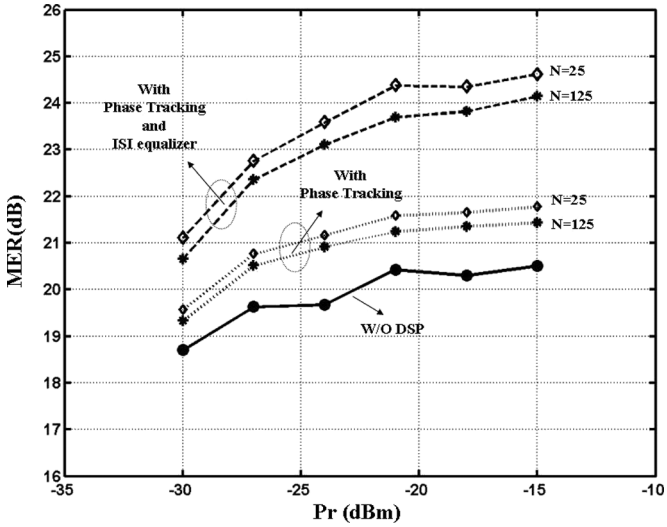

Fig. 14. Back-to-back MER dependence on the received optical power before the preamplifier.

for $\mathrm{N} = 125$. The later significantly simplifies the hardware implementation with a reduced clock rate of the digital signal processor with negligible MER penalty. As shown in Fig. 14, experimentally we obtained ~1 dB MER improvement through the phase tracking block.

The MER performance with both phase tracking block and ISI equalizer is shown in Fig. 14 for $\mathrm{N} = 125$ and $\mathrm{N} = 25$, respectively. The measured MER is 24.15 dB and 24.62 dB for $\mathrm{N} = 125$ and $\mathrm{N} = 25$, respectively, for $\mathrm{Pr} = -15$ dBm. The total MER improvement is ~3.5 dB for $\mathrm{N} = 125$, and ~4 dB for $\mathrm{N} = 25$ through the combination of phase correction and ISI equalization. The equalizer by itself improves the measured MER with ~2.7 dB, independent of N. This improvement is consistent with the simulation result. The measured signal constellation after the phase estimation block and the equalizer is shown in Fig. 15(a) and (15b), for $\mathrm{N} = 125$ and 25, respectively.

When ISI equalization and phase error tracking are both applied, the required received optical power before the optical amplifier is ~ −28 dBm to achieve $\mathrm{BER} = 10^{-9}$ (MER = 22.5 dB), according to Fig. 14. This received power level corresponds to ~2465 photons/bit for 5 Gbps data rate, and the

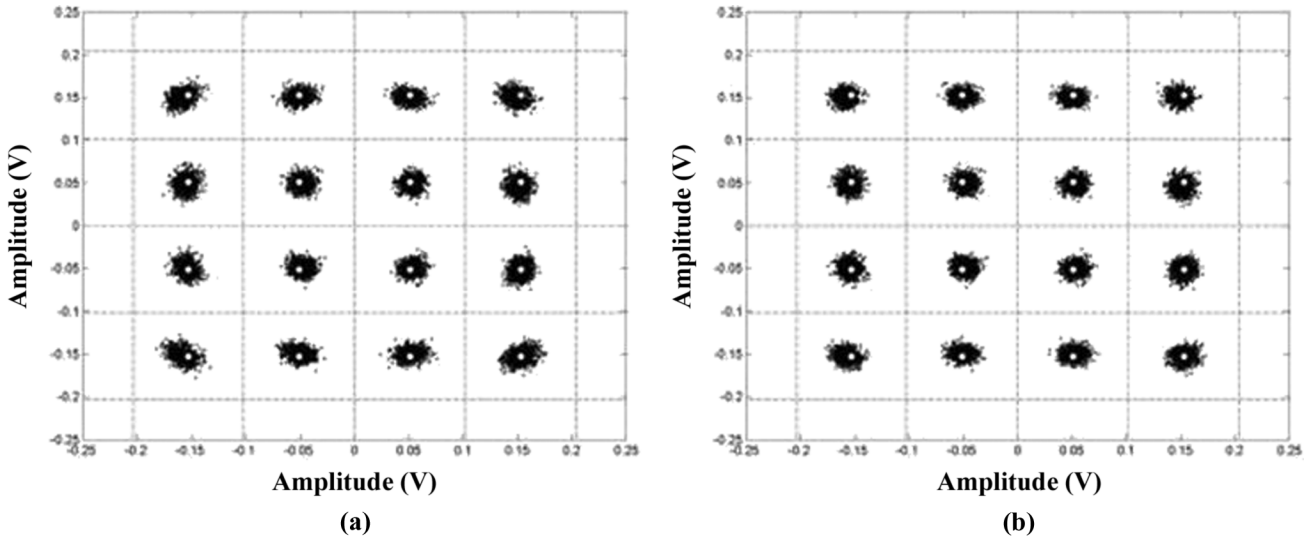

Fig. 15. Measured back-to-back signal constellation diagram with phase estimation and equalization. (a) For phase estimation block length of $\mathrm{N} = 125$. (b) For phase estimation block length of $\mathrm{N} = 25$.

penalty is 11.4 dB compared to the ASE-limited receiver sensitivity of 178 photons/bit.

In summary, the performance improvement (at $\mathrm{P_r} = -15\ \mathrm{dBm}$) through DSP blocks is shown in the following table.

	Without DSP	With Phase Tracking	With Phase tracking and ISI Equalizer
MER (dB)	20.58	21.44 (N=125)	24.15 (N=125)
		21.78 (N=25)	24.62 (N=25)

The DSP blocks are then applied to the stored data for unrepeated 100–km transmission experiment and the performance is compared with results obtained from a computer simulation using VPI. The simulation parameters of VPI were the same as the parameters used in the experiment Optical fiber loss $=$ 0.2 dB/km, optical fiber chromatic dispersion $= 17$ ps/nm, optical fiber nonlinear index $= 2.6 \times 10^{-20}$ m^2/w, and optical fiber core area $= 80\ \mu\mathrm{m}^2$, $\mathrm{f_{LO}} - \mathrm{f_{QAM}} = 20$ GHz, optical amplifier noise figure $= 6$ dB, modulation index $=$ 0.6, and the symbol length $= 1024 \times 16$ symbols. The MER was obtained with the combined use of VPI and Matlab. In the simulation, both the carrier phase recovery and frequency-response are assumed to be ideal, and only the fiber dispersion and nonlinear effects were considered. The simulation and experimental results (with DSP and $\mathrm{N} = 125$) for the 100 km system are shown in Fig. 16. Also shown in Fig. 16 is the back-to-back experimental performance after DSP improvement. The measured back-to-back MER was $\sim$24 dB, which is $\sim$4 dB improvement from the original back-to-back MER performance of 20 dB (shown in Fig. 10). The improvement, as mentioned previously, was due to $\sim$2.7 dB from ISI equalizer and $\sim$1 dB from phase error correction. However, comparing with the theoretical calculated $\mathrm{MER} = 31$ dB at $\mathrm{Pr} = -15$ dBm (see Fig. 10), there is still a MER penalty

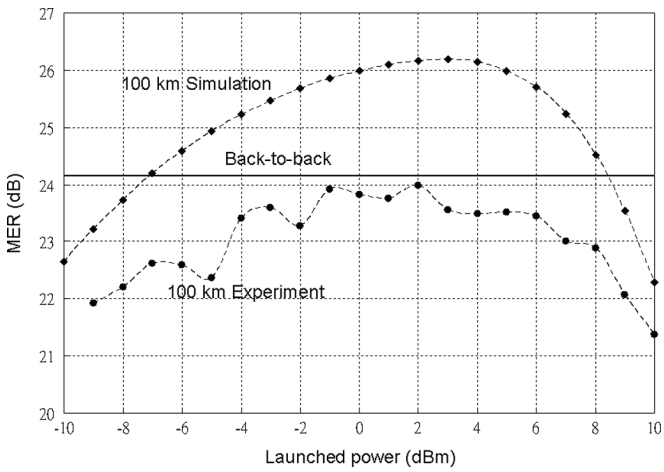

Fig. 16. Simulation and experimental results for unrepeated 100 km transmission after performance improvement through the DSP technique. The measured back-to-back MER is also shown.

of $\sim$7 dB (for $\mathrm{N} = 125$). The $\sim$7 dB penalty was due to the nonideal matched filter, ADC, frequency response, and the nonideal 4-PAM electrical signal generation (as can observed in Fig. 5).

In Fig. 16, the measured MER after phase error correction and ISI equalization for the 100–km transmission system, at an optimum fiber input power of 2 dBm, is 23.98 dB. This is about 2 dB lower than the simulation result. For higher and lower launched power levels than 2 dBm, the discrepancy between the measured and simulated MER is smaller, because in those power regions the nonlinear and ASE noise effects dominates over the ISI effect, respectively. Note that the reason why the measured MER is lower than the simulated ones by $\sim$2 dB is because of the residual back-to-back penalty that could not be compensated by the DSP blocks.

The measured constellations for a launched power of 2 dBm is essentially the same as that shown in Fig. 15(a). At a launched

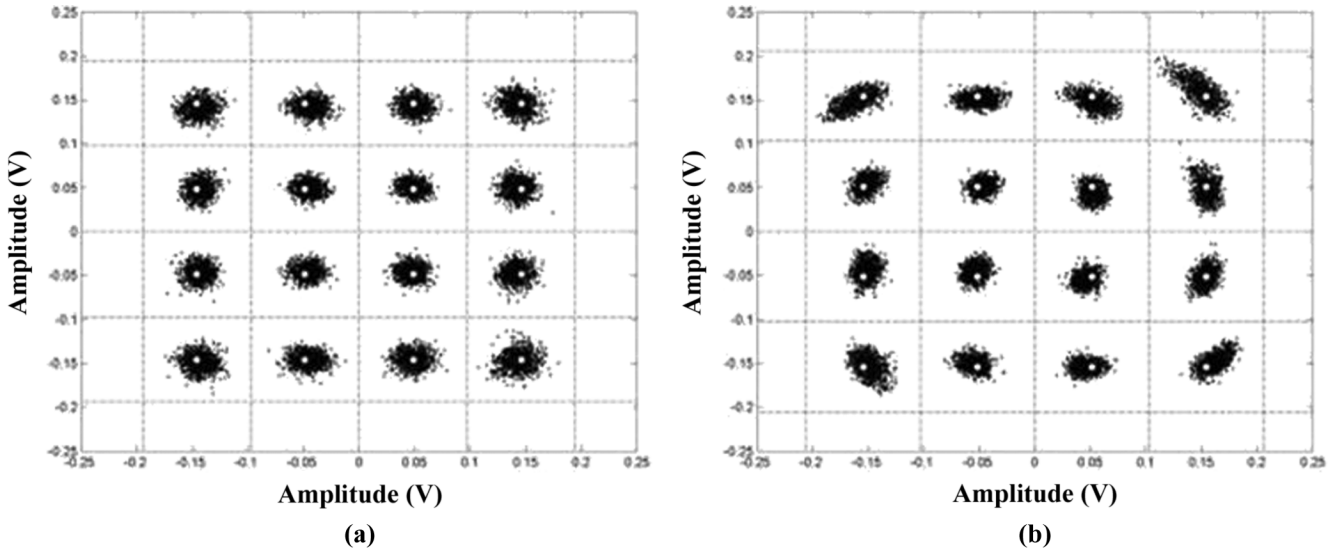

Fig. 17. Measured signal constellation diagram after unrepeated 100–km transmission with digital compensation. (a) For launched power of −9 dBm. (b) For launched power of 10 dBm.

power of −9 and 10 dBm, the constellation diagrams of the received signal after DSP are shown in Fig. 17(a) and (b), respectively. In Fig. 17(a), we can see that the noise is higher for the constellation points at the corners, which demonstrates the modulation amplitude-dependent noise due to Sig-Sp beat noise. In Fig. 17(b), there is an obvious phase rotation due to self-phase modulation (SPM) for constellation points at the edges. The phase tracking algorithm could not track the constellation well when the phase shift of the constellation points is intensity dependent.

VI. Conclusion

We have experimentally demonstrated a wideband 16QAM radio-over-fiber 100 km transmission system using a DSB-SC-based RSH technique, and evaluated the system performance analytically. It was concluded that the fundamental receiver sensitivity of the proposed technique is much better than conventional SCM systems, and is only 6 dB worse than a conventional coherent heterodyne system. We have also systematically identified sources of transmission system penalty, including phase noise, frequency response, optical amplifier noise, and fiber nonlinearity. We have observed ∼7 dB residual MER penalty even DSP was used to improve the back-to-back system performance, and believed that this large system penalty is caused by the nonideal ADC, digital matched filter, equalizer, and the nonideal generation of 4-PAM signal at the transmitter. A 64-QAM signal would be even more challenging because of the 6 dB higher OSNR requirement.

Appendix A
BER of Heterodyne ASK Detection in RSH System

Following (4), we have the IF signal at the photodetector output given by

$$S_{\mathrm{IF}}(t) = 2\mathrm{RGL}\sqrt{(2P_s)P_{\mathrm{LO}}}\cos(\omega_{\mathrm{IF}}t) + n(t) \text{ for bit "1"} \tag{A.1}$$

and

$$S_{\mathrm{IF}}(t) = n(t) \quad \text{for bit "0".} \tag{A.2}$$

Note that we have assumed that the single-sided noise density $\mathrm{N_0}$ for mark and space is the same and given by

$$N_0 = 2R^2\mathrm{GL}(P_S + P_{\mathrm{LO}})n_{\mathrm{eq}}(G-1)hf_0 \tag{A.3}$$

where we have assumed that the optical image rejection filter was used. After an ideal downconversion and a matched-filter detector, we obtain an output signal given by

$$S_D(t) = \frac{1}{T}\int_0^{T_b} S_{IF}(t)\cdot\sqrt{2}\cos(\omega_{IF}t)dt. \tag{A.4}$$

The SNR at the matched filter output is then described by [22]

$$SNR = \frac{S_{D\_1}^2 + S_{D\_0}^2}{\sigma_1^2 + \sigma_0^2} = \frac{4R^2G^2L^2P_SP_{LO} + 0}{N_0\frac{R_b}{2} + N_0\frac{R_b}{2}} = \frac{2LP_SP_{LO}}{(P_S + P_{LO})n_{eq}hf_0R_b} \quad \text{for G} \gg 1 \tag{A.5}$$

where S_{D_1} and S_{D_0} are the sampled signal of mark and space bit, respectively. For a fixed total transmission power $\mathrm{P_T} = \mathrm{P_S} + \mathrm{P_{LO}}$, the maximum SNR is achieved when $\mathrm{P_S} = \mathrm{P_{LO}} = \mathrm{P_T}/2$ and the resultant SNR is given by

$$\mathrm{SNR_{D\_ASK}} = \frac{\mathrm{LP_T}}{2\mathrm{n_{eq}hf_0R_b}}. \tag{A.6}$$

Assuming both mark and space have Gaussian conditional probability density functions with a decision threshold at

$\mathrm{RGL}\sqrt{P_S P_{\mathrm{LO}}}$, the BER of RSH ASK detection is then given by

$$\begin{aligned}\mathrm{BER} &= Q\left(\frac{\mathrm{RGL}\sqrt{P_S P_{LO}}}{\sqrt{N_0 \frac{R_b}{2}}}\right) \\ &= Q\left(\sqrt{\frac{L P_S P_{LO}}{(P_S + P_{LO}) n_{eq} h f_0 R_b}}\right) \quad \text{for } \mathrm{G} \gg 1 \quad \text{(A.7)}\end{aligned}$$

For $\mathrm{P_S} = \mathrm{P_{LO}} = \mathrm{P_T}/2$, the BER becomes

$$\begin{aligned}\mathrm{BER} &= Q\left(\sqrt{\frac{L P_T}{4 n_{\mathrm{eq}} h f_0 R_b}}\right) = \frac{1}{2} erfc\left(\sqrt{\frac{L P_T}{8 n_{\mathrm{eq}} h f_0 R_b}}\right) \\ &= \frac{1}{2} erfc\left(\sqrt{\frac{\mathrm{SNR_{D\_ASK}}}{4}}\right). \quad \text{(A.8)}\end{aligned}$$

REFERENCES

[1] G. H. Smith, D. Novak, and Z. Ahmed, "Overcoming chromatic-dispersion effects in fiber-wireless systems incorporating external modulators," *IEEE Trans. Microw. Theory Tech.*, vol. 45, no. 8, pt. 2, pp. 1410–1415, Aug. 1997.

[2] V. J. Urick, J. X. Qiu, and F. Bucholtz, "Wide-band QAM-over-fiber using phase modulation and interferometric demodulation," *IEEE Photon. Technol. Lett.*, vol. 16, no. 10, pp. 2374–2376, Oct. 2004.

[3] M. A. Piqueras, B. Vidal, J. L. Corral, V. Polo, A. Martinez, and J. Marti, "Direct photonic generation of electrical vector modulations at microwave/millimeter-wave frequencies," *IEEE Photon. Technol. Lett.*, vol. 17, no. 9, pp. 1947–1949, Sep. 2005.

[4] J. Hongo, K. Kasai, M. Yoshida, and M. Nakazawa, "1-Gsymbol/s 64-QAM coherent optical transmission over 150 km," *IEEE Photon. Technol. Lett.*, vol. 19, no. 9, pp. 638–640, May 2007.

[5] K. P. Ho and H. W. Cuei, "Generation of arbitrary quadrature signals using one dual-drive modulator," *J. Lightw. Technol.*, vol. 23, no. 2, pp. 764–770, Feb. 2005.

[6] M. Seimetz, "Performance of coherent optical square-16-QAM-systems based on IQ-transmitters and homodyne receivers with digital phase estimation," in *Proc. OFC 2006 and 2006 NFOEC*, 2006, NWA4.

[7] E. Ip and J. M. Kahn, "Carrier synchronization for 3- and 4-bit-per-symbol optical transmission," *J. Lightw. Technol.*, vol. 23, no. 12, pp. 4110–4124, Dec. 2005.

[8] R. Hofstetter, H. Schmuck, and R. Heidemann, "Dispersion effects in optical millimeter-wave systems using self-heterodyne method for transport and generation," *IEEE Trans. Microw. Theory Tech.*, vol. 43, no. 9, pp. 2263–2269, Sept. 1995.

[9] U. Gliese, T. N. Nielsen, S. Norskov, and K. E. Stubkjær, "Multifunctional fiber-optic microwave links based on remote heterodyne detection," *IEEE Trans. Microw. Theory Tech.*, vol. 46, no. 5, pt. 1, pp. 458–468, May 1998.

[10] J. D. Gaudette, D. J. Krause, J. C. Cartledge, and K. Roberts, "Offset sideband modulation at 2.5 GSym/s," in *Proc. Optical Fiber Commun. Conf.*, Anaheim, CA, 2007, OThD1.

[11] R. Montgomery and R. Desalvo, "A novel technique for double sideband suppressed carrier modulation of optical fields," *IEEE Photon. Technol. Lett.*, vol. 7, no. 4, pp. 434–436, Apr. 1995.

[12] S. Shimotsu, S. Oikawa, T. Saitou, N. Mitsugi, K. Kubodera, T. Kawanishi, and M. Izutsu, "Single side-band modulation performance of a $\mathrm{LinbO_3}$ integrated modulator consisting of four-phase modulator waveguides," *IEEE Photon. Technol. Lett.*, vol. 13, no. 4, pp. 364–366, Apr. 2001.

[13] R. A. Griffin, P. M. Lane, and J. J. O'Reilly, "Optical amplifier noise figure reduction for optical single-sideband signals," *J. Lightw. Technol.*, vol. 17, no. 10, pp. 1793–1796, Oct. 1999.

[14] G. P. Agrawal, *Fiber-Optic Communication Systems*, 2nd ed. New York: Wiley-Intersci., 1997.

[15] L.-L. Yang and L. Hanzo, "A recursive algorithm for the error probability evaluation of M-QAM," *IEEE Commun. Lett.*, vol. 4, no. 10, pp. 304–306, Oct. 2000.

[16] J. M. Kahn and K.-P. Ho, "Spectral efficiency limits and modulation/detection techniques for DWDM systems," *IEEE J. Sel. Topics Quantum Electron.*, vol. 10, no. 2, pp. 259–272, Mar./Apr. 2004.

[17] D. S. Ly-Gagnon, S. Tsukamoto, K. Katoh, and K. Kikichi, "Coherent detection of optical quadrature phase-shift keying signals with carrier phase estimation," *J. Lightw. Technol.*, vol. 24, no. 1, pp. 12–21, Jan. 2006.

[18] S. Waklin and J. Conradi, "Multilevel signaling for increasing the reach of 10 Gb/s lightwave systems," *J. Lightw. Technol.*, vol. 17, no. 11, pp. 2235–2248, Nov. 1999.

[19] H. Meyr, M. Moeneclaey, and S. A. Fechtel, *Digital Communication Receivers: Synchronization, Channel Estimation, and Signal Processing*. New York: Wiley, 1998.

[20] S. Haykin, *Adaptive Filter Theory*, 4th ed. Englewood Cliffs, NJ: Prentice-Hall, 2002.

[21] P. Y. Kam, "Maximum likelihood carrier phase recovery for linear suppressed-carrier digital data modulations," *IEEE Trans. Commun.*, vol. COM-34, no. 6, pp. 522–527, June 1986.

[22] J. G. Proakis, *Digital Communications*, 4th ed. New York: McGraw-Hill Int., 2001.

Chia-Kai Weng was born in Ping-Tong, Taiwan, R.O.C., in 1975. He received the B.S. and M.S. degrees from National Chiao-Tung University, Taiwan, in 1997 and 1999, respectively.

He is currently working toward the Ph.D. degree at the same institution. His current interests include digital signal processing in coherent optical communications and performance analysis of radio-over-fiber systems.

Yu-Min Lin received the B.S. degree in electrical engineering from National Tsing-Hua University, Hsinchu, Taiwan, R.O.C., in 1996 and the Ph.D. degree in communications engineering from National Chiao-Tung University, Hsinchu, Taiwan, in 2003.

He joined the Department of Optical Communications and Networks, Information and Communication Laboratories, Industrial Technology Research Institute (ITRI/ICL), Taiwan, in 2004. His research interests include transmission technologies in optical fiber communications and broadband access system.

Winston I. Way (S'82–M'82–SM'88–F'01) received the M.S. and Ph.D. degrees from the University of Pennsylvania, Philadelphia, in 1981 and 1983, respectively.

He was with Applied Research, Bellcore (now Telcordia), Red Bank, NJ, from 1984 to 1992, where he pioneered research in subcarrier-multiplexed lightwave systems and conducted a number of front-end dense-wavelength-division-multiplexing (DWDM) digital/analog video transmission experiments. From 1992 to 2000, he was a Professor with the National Chiao-Tung University, Hsinchu, Taiwan, R.O.C., where he continued leading a number of research projects in HFC systems and networks. From 1998 to 2000, he was also a Consultant with Telcordia, conducting research on next-generation Internet optical networks. In 2000, he founded OpVista Inc., Milpitas, CA, and has been developing ultra-DWDM transmission equipment. He is the author of the book *Broadband Hybrid/Fiber Coax System Technologies* (New York: Academic, 1998), has published more than 100 journal and conference papers, and holds 20 U.S. and European patents.

Dr. Way has served on the technical program committees of OFC, ECOC, IEEE MTT, OECC, and the IEEE Lasers and Electro-Optics Society (LEOS).